Proceedings of the 20th International Conference on Soil Mechanics and Geotechnical Engineering– Rahman and Jaksa (Eds)

Experimental study on the particle breakage of calcareous sand

Étude expérimentale sur la fragmentation des particules de sable calcaire

Li Cheng
South China Institute of Geotechnical Engineering, School of Civil Engineering and Transportation, South China University of Technology, China, licheng_scut@126.com

Muhammad Shazzad Hossain & Youngho Kim
Centre for Offshore Foundation Systems, Oceans Graduate School, The University of Western Australia, Australia

Yuxia Hu
School of Civil, Environmental and Mining Engineering, The University of Western Australia, Australia

Shah Neyamat Ullah
School of Engineering and Technology, Central Queensland University Australia, Australia

ABSTRACT: This paper reports the results from a series of triaxial compression tests undertaken to provide insight into the particle breakage of a calcareous sand. The effects of relative density, confining pressure and axial strain on the evolution of particle breakage were investigated. The degree of particle breakage was measured by comparing the particle size distribution (PSD) before and after each test, leading to develop a modified particle breakage index. The results show that more particle breakage occurs in denser samples and for higher confining pressure. With the increase of axial strain, the rate of particle breakage increases first and then decreases. The evolution of particle breakage is demonstrated linking with normalised mean effective stress and shearing strain. The results can be used in predicting the mobilised friction angle and therefore sand strength including the influence of particle breakage.

RÉSUMÉ: Les résultats d'une série d'essais de compression triaxiale ont été rapportés dans le but de révéler la fragmentation des particules de sable calcaire.Les effets de la densité relative, de la pression de confinement et de la déformation axiale sur l'évolution de la fragmentation des particules ont été étudiés.Le degré de fragmentation des particules a été mesuré en comparant la distribution granulométrique (PSD) avant et après chaque essai afin d'obtenir un nouvel indice de fragmentation des particules modifié.Les résultats montrent que plus la densité est élevée, plus la pression de confinement est élevée et plus la fragmentation des particules est grave.Avec l'augmentation de la déformation axiale, la fragmentation des particules augmente d'abord puis diminue.L'évolution de la fragmentation des particules est reliée à la contrainte normale et à la déformation de cisaillement.Les résultats peuvent être utilisés pour prédire l'angle de frottement dynamique et donc la résistance du sable, y compris l'effet de la fragmentation des particules.

KEYWORDS: calcareous sand, triaxial tests, particle breakage, friction angle

1 INTRODUCTION

Calcareous sediments cover more than 40% of the seabed, including the continental shelf and coastline of tropical or subtropical regions (Holmes, 1978). As such, calcareous soils are prevalently encountered in many oil and gas producing regions and in areas for potential renewable energy developments (Watson et al. 2019). Calcareous sands are formed through biogenic primary production and/or authigenic precipitation, and its material compositions mainly originate from shells, corals, and biological debris (Zhou et al. 2018). Therefore, they typically have low grain hardness, large intra-granular porosity, wider range of grain shapes and angularity, and more complex structural arrangements. These characteristics reflect unique post-depositional processes of cementation, dissolution, recrystallisation, and other diagenetic changes (He et al. 2020, Zhang et al. 2020). The unique nature can have significant influence on offshore foundation design processes from concept stage to operation, and ultimately to decommissioning (Watson et al. 2019). Thus, a better understanding of these sediments, in terms of the mechanical behaviour, is important to reduce the uncertainties in offshore foundation designs.

Many laboratory tests, such as one-dimensional compression tests (Altuhafi & Coop 2011, Al Hattamleh et al. 2013, Xiao et al. 2017), triaxial compression tests (Coop et al. 2004, Hassanlourad et al. 2008, Shahnazari & Rezvani 2013, Ghafghazi et al. 2014, Yu 2017a, 2017b, Yu 2019, Wang et al. 2019, Liu et al. 2020, Zhang & Luo 2020) and ring shear tests (Simoni & Houlsby 2006, Brandes 2011, Wei et al. 2018) were conducted to investigate the effect of particle breakage on the mechanical behaviour of calcareous sand. By conducting a series of triaxial tests, Yu (2017a) and Liu et al. (2020) have found that particle breakage tends to increase with increasing stress level and sand relative density. Yu (2017a) conducted a series of drained triaxial tests on pre-crushed material, and reported that the peak friction angle and dilation angle decrease due to particle breakage, and the critical state angle increases to a peak value and then decrease with increasing particle breakage. However, Coop et al. (2004) showed that the critical state friction angle remains nearly unchanged regardless of amount of particle breakage in ring shear tests. Recently, based on triaxial test results, Wang et al. (2020) concluded that particle breakage generally increases with increasing axial strain and continues to increase even after reaching the peak deviatoric stress.

Under the traditional triaxial loading conditions for sand, Rowe (1962) developed the following stress–dilatancy relationship:

$$\frac{\sigma_1'}{\sigma_3'} = \left(1 - \frac{d\varepsilon_v}{d\varepsilon_1}\right)\tan^2\left(45° + \frac{\phi_\mu}{2}\right) \quad (1)$$

where σ'_1 is the major principal stress and σ'_3 is the minor principal stress, $d\varepsilon_v$ is the volumetric strain increment (compression is taken as positive), $d\varepsilon_1$ is the axial strain increment (compression is positive) and ϕ_μ is the true friction angle. The stress ratio σ'_1/σ'_3 essentially represents the deviatoric stress q. However, this expression is only suitable for silica sand, and the effect of particle breakage was not considered. For crushable soils, Ueng and Chen (2000) modified Rowe's stress–dilatancy relationship according to:

$$\frac{\sigma_1^{'}}{\sigma_3^{'}} = \left(1 - \frac{d\varepsilon_v}{d\varepsilon_1}\right)\tan^2\left(45° + \frac{\phi_f}{2}\right) + \frac{dE_B}{\sigma_3 d\varepsilon_1}\left(1 + \sin\phi_f\right) \qquad (2)$$

where ϕ_f is the friction angle excluding dilation and particle breakage, and dE_B is the energy consumption related to grain crush. The second term on the right side of Eq. 2 corresponds to particle breakage. ϕ_f was used instead of ϕ_μ to consider the basic friction angle and energy spent on the process of rearrangement of the particle assembly. Based on some triaxial test results, Ueng & Chen (2000) found that the particle breakage angle (contributed by the energy consumption due to particle breakage) increases with increasing confining pressure and relative density.

In this study, the effects of influencing parameters including confining pressure, relative density and axial strain on particle breakage of a calcareous sand (i.e. Ledge Point sand, see next section) were examined. A series of drained triaxial compression tests was conducted varying the influencing parameters. Particle size distribution (PSD) analyses were performed before and after each test, and the particle breakage values were calculated using a modified method based originally on Hardin (1985).

2 SOIL CHARACTERISATION

The experimental program was conducted in the Soil Mechanics Laboratory at the University of Western Australia (UWA). The experimental set-up is shown in Figure 1.

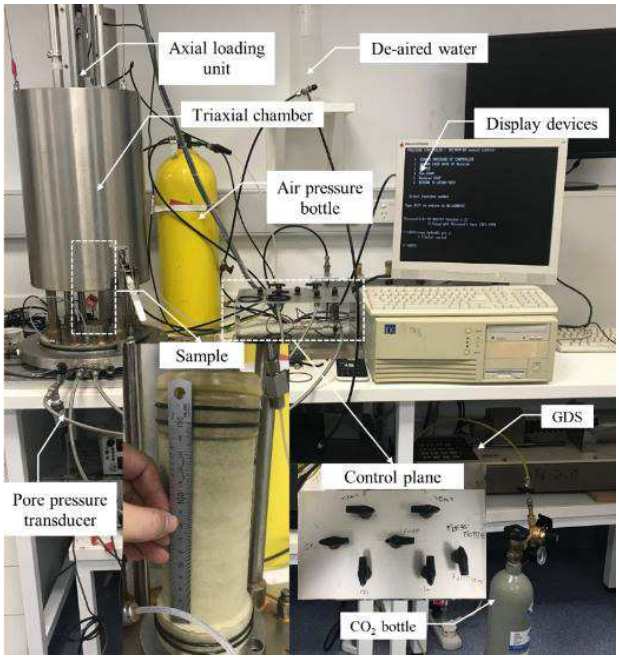

Figure 1. Typical test set-up in triaxial apparatus at UWA

Calcareous sand material was collected from Ledge Point, Western Australia (Sharma & Ismail 2006, Teng et al. 2019). The initial particle size distribution (PSD) of the sand is shown in Figure 2. It can be inferred from the gradation curve that the selected soil is a poorly graded sand (i.e. uniform grading). Figure 3 displays a scanning electron microscopic (SEM) image, showing that the sand was dominated by porous and irregularly shaped particles.

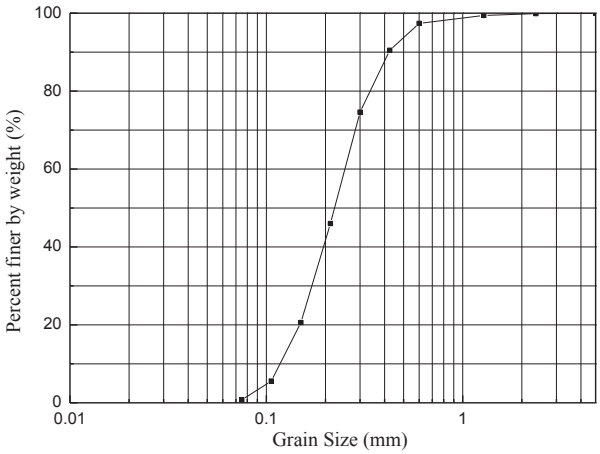

Figure 2. Initial particle size distribution (PSD) of Ledge Point sand

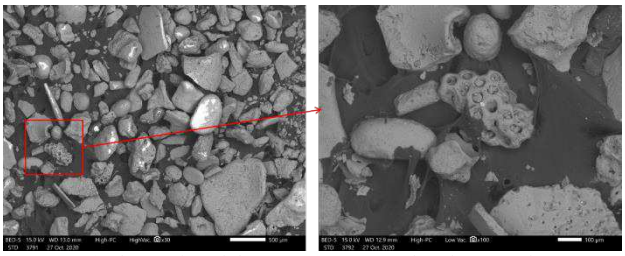

(a) Shape of particles (b) Close-up view

Figure 3. SEM image of Ledge Point sand

The carbonate content ($CaCO_3$) of the sand was 93%, as was determined using the acid dilution method (WA 915.1, 2012). Table 1 lists the key physical properties of the sand.

The critical state friction angle, ϕ'_{cv}, was determined by conducting triaxial tests on loose specimens. The results showed that ϕ'_{cv} = ~36.1 degrees, which is significantly higher than silica sands. This is due to the larger intrinsic friction angle and the angular shape of the soil particles (Lehane et al. 2014).

Table 1 Physical properties of Ledge Point sand

Property	Values
Carbonate content: %	93.0
Specific gravity, G_s: -	2.74
Max void ratio, e_{max}: -	1.19
Min void ratio, e_{min}: -	0.80
d_{50}: mm	0.22
Uniformity coefficient, C_u: -	2.14

3 SAMPLE PREPARATION AND TESTING PROCEDURE

A typical monotonic triaxial test can be divided into four steps: sample preparation, saturation, consolidation and shearing. In addition, a PSD analysis was carried out after each test. The specimens were 70.8 mm in diameter and 139 mm in height. A 1.2 mm thick membrane was adopted to preclude perforation by the angular particles of the sand and to reduce penetration. Before sample preparation, the sample quantity was determined based on the water content, size and relative density of the sample. The sample was compacted in eight layers to maintain the uniformity

along the height, while achieving the desired density. The quantity of each layer increases linearly with the height of the sample and the top layer has a 5% more mass than the bottom layer to obtain a uniform density sample. Due to the numerous inner pores contained in the sand, it was difficult to saturate the samples, as was also experienced by others (e.g. Wang et al. 2019). A fully saturation condition of the specimens was achieved through three stages. First, CO_2 was flushed to the specimen for 20 mins; second, de-aired water exuded to the specimen; finally, a back pressure of 600 kPa under an effective pressure of approximately 20 kPa was applied. Using this method, all specimens have achieved high saturation conditions, and Skempton's B_s values were greater than 0.95 under isotropic consolidation.

Drained triaxial compression tests were then carried out under various confining pressures of 100~500 kPa. The vertical loading was applied by pushing the ram vertically downward at a rate of 0.1 mm/min. Under the isotropic consolidation condition ($\varepsilon_1 = 0$), the PSD curve after the consolidation was found to be very similar to the original one (Yu 2019) i.e. particle breakage was minimal. For tests under a confining pressure, a full compression test was conducted till the axial strain reaching $\varepsilon_1 = 33\%$. The axial strain at the peak deviatoric stress was identified as ε_f. Three subsequent tests under the same confining pressure were then conducted up to various axial strain levels (i.e. stopping the tests on purpose at axial strain levels) of $\varepsilon_1 = 0.5\varepsilon_f$, ε_f and 20%.

At the end of each test, the whole material of the tested specimen was put in the refrigerator to record the saturated sample mass; and then the sample was dried in an oven to record the dry sample mass. After drying, the materials were washed on a 0.075 mm sieve and dried again to obtain the mass of the finer particles, hence the particle size distribution (PSD) after shearing.

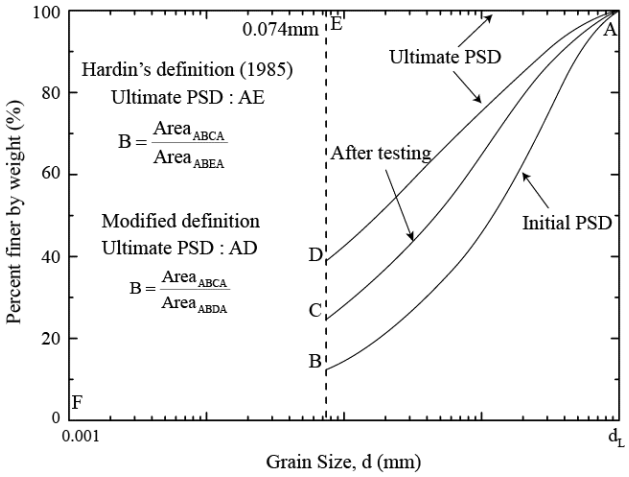

Figure 4. Definition of modified particle breakage index

To quantify particle breakage, a number of particle breakage indexes have been proposed, mostly measuring grade changes before and after shearing (Hardin 1985, Lade et al. 1996, Einav 2007a, 2007b, Kikumoto et al. 2010, Yu 2018). Hardin (1985) proposed a special procedure based on the overall particle size distribution. This method has been accepted by many researchers in their studies (Luzzani & Coop 2002, Coop et al. 2004, Yu 2019). The 100% finer line has been defined as the ultimate PSD line (i.e. AE line in Figure 4). However, there is no experimental support for achieving 100% breakage even under a very high pressure (Coop et al. 2004). As such, for a more achievable ultimate PSD curve, the expression below was adopted in this study.

$$F_u = \left(\frac{d}{d_L}\right)^{3-\alpha_1} \tag{3}$$

where α_1 is a fractal dimension (= 2.6 for uniformly graded sand; Einav, 2007a), d is the size of the particles, d_L is the largest particle size and F_u is the function of the ultimate PSD curve. To fit with non-uniformly graded Ledge Point sand, $\alpha_1 = 2.8$ was considered. The ultimate PSD line was considered as AD, and an according modified breakage index was proposed, as shown in Figure 4.

4 TRIAXIAL TEST RESULTS

4.1 *Stress-strain response and volumetric change*

A total of 21 triaxial compression tests were performed under consolidated drained (CD) conditions. In order to quantify the corresponding influence on the evolution of particle breakage, a range of confining pressure (σ'_3: 100~500kPa), relative density (D_r: 55~75%) and axial strain (ε_1: 4~33%) were considered. A series of parallel tests along the same loading path were conducted on the specimens of the same initial density and confining pressure, but the tests were terminated at different axial strains, as noted previously.

Typically, Figure 5 shows the results for confining pressure $\sigma'_3 = 300$ kPa and relative density $D_r = 75\%$. The curves show softening and dilative behaviour after initial hardening and contraction. The rate of post-peak reduction of deviatoric stress q and volumetric strain ε_v reduces steadily with increasing axial strain, leading to the critical state. This slow change in the response was due to the interaction between particle breakage and dilation of the sand. Similar results from triaxial tests were reported by Wang et al. (2020).

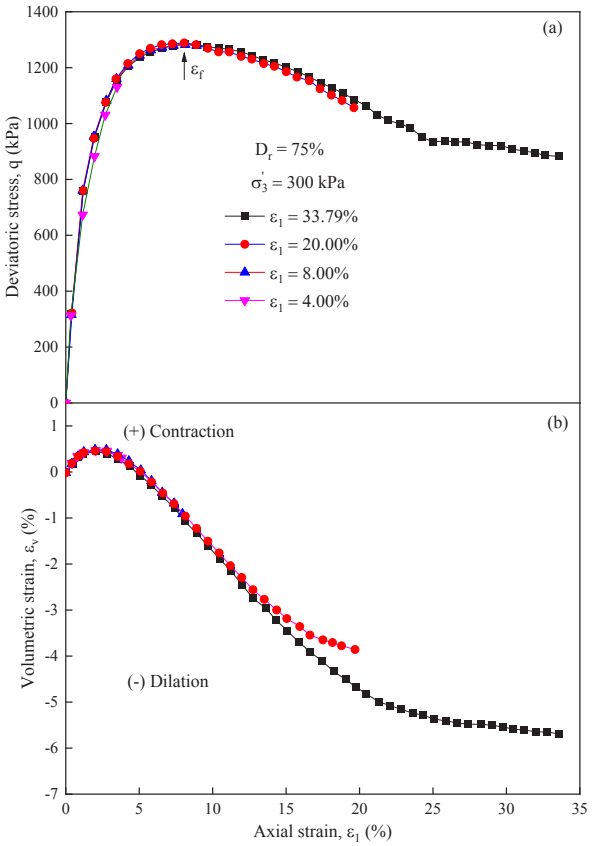

Figure 5. Typical test results: (a) Axial stress–strain response; (b) Volumetric change

Figure 6 shows the values of σ'_1/σ'_3 at failure or at peak deviatoric tress, $(\sigma'_1/\sigma'_3)_f$, as a function of the dilatancy factor at peak deviatoric stress, $(1 - d\varepsilon_v/d\varepsilon_1)_f$. It appears that the stress ratio for the calcareous sand increases linearly with dilatancy. The triaxial test data on decomposed granite reported by Miura & Sukeo (1979) and on Fulung sand and Tamsui River sand published in Ueng & Chen (2000) are also plotted in Figure 6 for comparison. However, since those results included the effect of different relative densities and the amount of particle breakage under different confining pressures, this is obviously not Rowe's stress–dilatancy relationship (Eq. 1; Ueng & Lee, 1990, Ueng & Chen 2000).

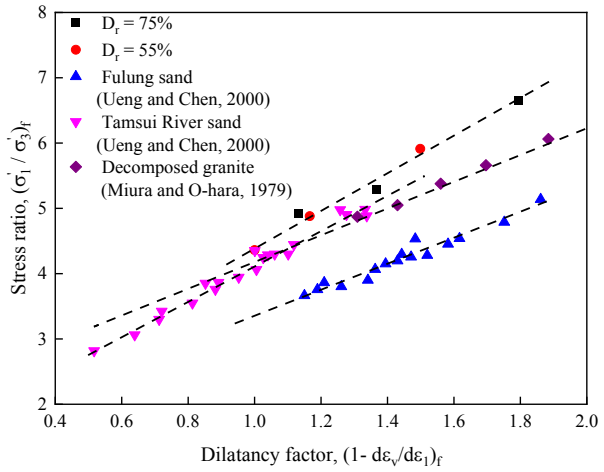

Figure 6. Influence of dilatancy on stress ratio at peak deviatoric stress

In the triaxial compression test, the peak friction angle, ϕ_p, and the peak dilation angle, ψ_p, can be calculated as:

$$\sin\phi_p = \left[\frac{\sigma'_1/\sigma'_3 - 1}{\sigma'_1/\sigma'_3 + 1}\right]_p \quad (5)$$

$$\sin\psi_p = -\left[\frac{d\varepsilon_1/2 + d\varepsilon_3}{d\varepsilon_1/2 - d\varepsilon_3}\right]_p \quad (6)$$

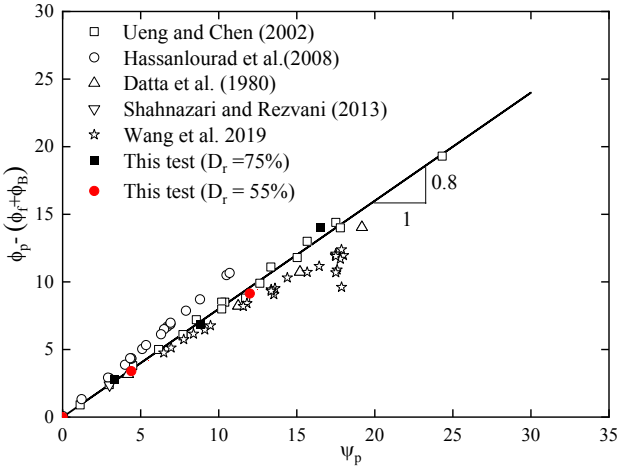

Figure 7. Variation of $\phi_p - (\phi_f + \phi_B)$ with peak dilation angle ψ_p

Using Eqs. 5 and 6 and the data of $(\sigma'_1/\sigma'_3)_f$ and $(1 - d\varepsilon_v/d\varepsilon_1)_f$ and assuming $dE_B = 0$ in Eq. 2; $(\phi_f + \phi_B)$ can be obtained, which includes friction angle ϕ_f and particle breakage angle ϕ_B due to the crushing of particles, more details can be found in Ueng & Chen (2000). Figure 7 shows the variation of $\phi_p - (\phi_f + \phi_B)$ with peak dilation angle ψ_p. The triaxial test data on decomposed granite (sand size) reported by Miura & Sukeo (1979); on Fulung sand and Tamsui River sand presented by Ueng & Chen (2000); and on calcareous sands published by Datta et al. (1980), Hassanlourad et al. (2008), Shahnazari & Rezvani (2013) and Wang et al. (2019) are also included in Figure 7 for comparison. As shown in Figure 7, the best fit through the data provides the below relationship allowing predicting the peak operative friction angle for breakable sand:

$$\phi_p = \phi_f + \phi_B + 0.8\psi_p \quad (7)$$

4.2 *Evolution of particle breakage in triaxial tests*

As noted previously, for assessing the evolution of particle breakage tests were terminated at various axial strain levels, and PSD was determined. Figure 8 shows the PSD curves for relative density D_r = 75% and confining pressure σ'_3 = 300 kPa. The gap between the initial PSD curve and those after shearing is widened with increasing axial strain. This gap represents the particle breakage. Based on the proposed modified definition in Figure 4 and Eq. 3, particle breakage index (B) was calculated.

Coop et al. (2004) undertaken a series of ring shear tests on Dogs Bay sand. They showed that particle breakage continued until attaining the critical state at very large strains between 2000% and 10000%. They concluded that the critical states observed in triaxial tests on crushable soils were only transient constant-volume states and that true critical states were achieved only at very high strains when all crushing have ceased. However, they also showed that a friction angle of the same magnitude as that reached under the critical state condition was mobilised at a shear strain of only about 30%. In most geotechnical applications, soil does not reach very large strains (Kan & Taiebat 2014).

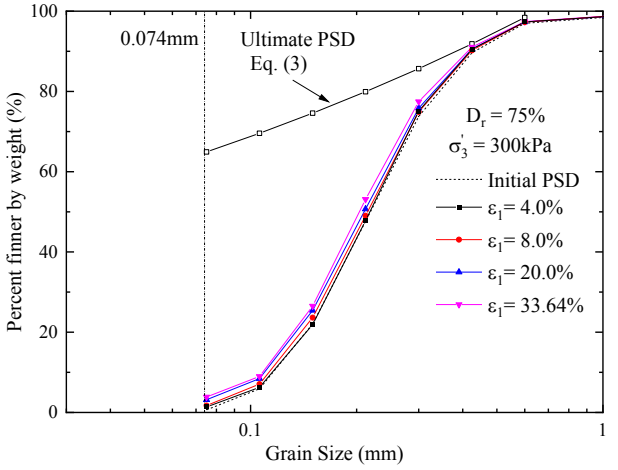

Figure 8. Particle size distribution (PSD) curves for various axial strains (D_r = 75%, σ'_3 = 300 kPa)

In the current triaxial test, the maximum shearing strain was limited to ~33%. For dense and medium dense sands, it is difficult to reach the critical state in triaxial tests due to the apparatus limitation. Therefore, it was assumed that the critical state was achieved at an axial strain of ~33%.

Hardin (1985) suggested that the volumetric strain would cease only when particle breakage stopped and a stable grading was achieved. The critical state represents a balance between volumetric compression arising from particle breakage and volumetric dilation from the particle rearrangement (Baharom & Stallebrass 1998). After reaching the critical state, volumetric strain remains constant, and so does the particle breakage index, B_{cv}.

Figure 9 plots the values of B_{cv} as a function of normalised mean effective stress. It can be seen that particle breakage at critical state increases with the increase of normalised mean effective stress. The denser the sand is, the greater the amount of particle breakage occurs at the critical state.

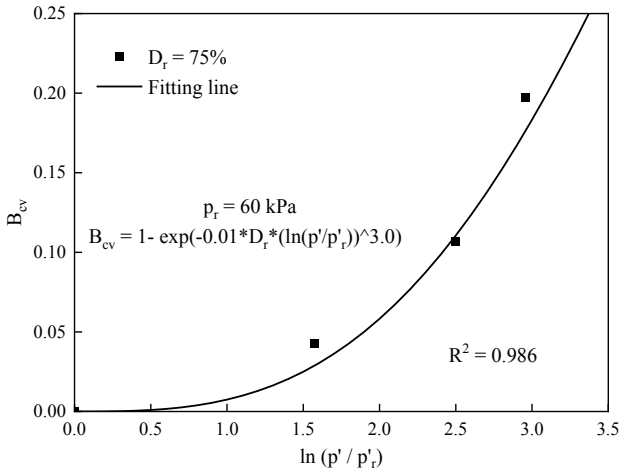

Figure 9. Typical variation of particle breakage index at critical state B_{cv} with normalised mean effective stress (D_r = 75%, σ'_3 = 300 kPa)

The particle breakage at critical state may be presented by a single nonlinear function as:

$$B_{cv} = 1 - \exp(-\lambda * D_r * (\ln(p^{'} / p_r^{'}))^{\alpha_2}) \quad (8)$$

where λ and α_2 are two material constants relating to the breakage of particles. p'_r is defined as a reference pressure. The particles begin to crush when the mean effective stress p' exceeds the reference pressure p'_r. Best fit through the data in Figure 9 provides λ = 0.01, α_2 = 3.0 and p'_r = 60 kPa.

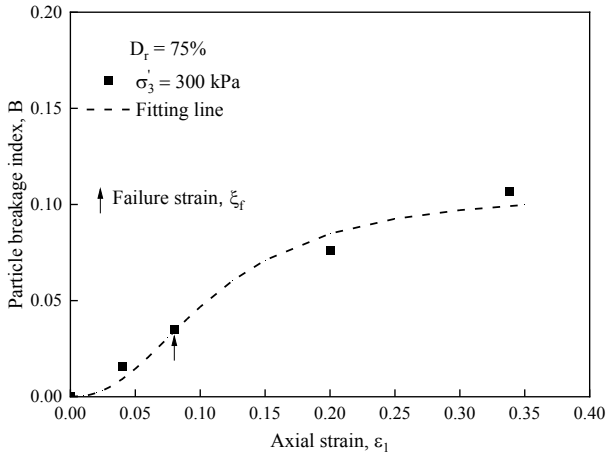

Figure 10. Evolution of particle breakage B with axial strain (D_r = 75%, σ'_3 = 300 kPa)

Figure 10 shows the evolution of particle breakage index B as a function of axial strain ε_1. The failure strain (ε_f) is indicated on the plot, and the locus of the failure strain is also shown. The degree of particle breakage increases with the increase of axial strain. It was also found that B increases with confining pressure and relative density, which is consistent with the results presented by Yu (2018b). There is no particle breakage and the rate of particle breakage is zero when $\varepsilon_f = 0$. Before reaching the failure strain ($\varepsilon_1 < \varepsilon_f$), B and the rate of particle breakage increase with deviatoric stress. At the failure strain ($\varepsilon_1 = \varepsilon_f$), the rate of particle breakage reaches the maximum due to the peak deviatoric stress.

Particle breakage continues to increase even after the peak deviatoric stress. The rate of particle breakage decreases with increasing axial strain, but increases with increasing confining pressure, which is consistent with test results published by Indraratna & Salim (2002) and Liu & Zou (2013).

From the plots of B_{cv} versus ε_1 and the plot of B versus ε_1, particle breakage of the Ledge Point sand in triaxial tests may be expressed according to:

$$B = \begin{cases} \dfrac{B_{cv}}{1+10^{\chi - \ln(\theta\varepsilon_1)}}, & \varepsilon_1 \le \varepsilon_{cv} \\ B_{cv}, & \varepsilon_1 > \varepsilon_{cv} \end{cases} \quad (9)$$

where χ and θ are the material constants defining the shape of the particle breakage curve. Calibrating Eq. 6 with the data in Figure 10, the values can be found as χ = 0.13, θ = 10.0.

5 CONCLUSIONS

Particle breakage dictates the mechanical behaviour of calcareous sands. A series of triaxial compression tests were conducted to investigate the effects of critical parameters; confining pressure, relative density, axial strain; on particle breakage of the Ledge Point calcareous sand. The amount of particle breakage was measured from the PSD curves before and after each test at various axial strain levels. Modified particle breakage index B and particle breakage index at critical state B_{cv} were calculated. The following conclusions can be inferred from the results presented:

1. Particle breakage and rate of particle breakage increased with increasing confining pressure.

2. Under the same axial strain and confining pressure, particle breakage and the rate of particle breakage were higher for denser sand.

3. The amount of particle breakage increased with the increase of axial strain, but the rate of particle breakage first increased and then decreased with the increase of axial strain.

4. Modified particle breakage index B and particle breakage index at critical state B_{cv} can be assessed using Eqs. 9 and 8, respectively. These equations can be linked to the mobilised friction angle hence allowing sand strength and volumetric deformation to be predicted using analytical and numerical methods.

6 ACKNOWLEDGEMENTS

The triaxial compression tests were performed during the lead author's visit to the University of Western Australia. His visit was supported by the Natural Science Foundation of Guangdong Province (No. 2020A1515010745) and the Fundamental Research Funds for the Central Universities (No. 2019MS119). The second author is an ARC Future Fellow and is supported by the ARC Project FT190100735. This support is gratefully acknowledged.

7 REFERENCES

Al Hattamleh, O.H., Al-Deeky, H.H. and Akhtar, M.N. 2013. The consequence of particle crushing in engineering properties of granular materials. *International Journal of Geosciences*.

Altuhafi, F.N. and Coop, M.R. 2011. Changes to particle characteristics associated with the compression of sands. *Géotechnique* 61(6), 459-471.

Baharom, B. and Stallebrass, S. 1998. A constitutive model combining the microscopic and macroscopic behaviour of sands in shear and volumetric deformation. *In Application of Numerical Methods to Geotechnical Problems.)*, Springer, 263-272.

Brandes, H. 2011. Simple shear behavior of calcareous and quartz sands. *Geotechnical and Geological Engineering* 29(1),113-126.

Coop, M.R., Sorensen, K.K., Freitas, T.B. and Georgoutsos, G. 2004. Particle breakage during shearing of a carbonate sand. *Géotechnique* 54(3), 157-163.

Datta, M., Gulhati, S.K. and Rao, G.V. 1980. Crushing of calcareous sands during drained shear. *Society of Petroleum Engineers Journal* 20(2), 77-85.

Einav, I. 2007a. Breakage mechanics - Part I: Theory. *Journal of the Mechanics and Physics of Solids* 55(6), 1274-1297.

Einav, I. 2007b. Breakage mechanics - Part II: Modelling granular materials. *Journal of the Mechanics and Physics of Solids* 55(6), 1298-1320.

Ghafghazi, M., Shuttle, D.A. and Dejong, J.T. 2014. Particle breakage and the critical state of sand. *Soils and Foundations* 54(3), 451-461.

Hardin, B.O. 1985. Crushing of Soil Particles. *Journal of Geotechnical Engineering, ASCE*, 111(10), 1177-1192.

Hassanlourad, M., Salehzadeh, H. and Shahnazari, H. 2008. Dilation and particle breakage effects on the shear strength of calcareous sands based on energy aspects. *International Journal of Civil Engineering* 6(2), 108-119.

He, S.-H., Ding, Z., Xia, T.-D., Zhou, W.-H., Gan, X.-L., Chen, Y.-Z. and Xia, F. 2020. Long-term behaviour and degradation of calcareous sand under cyclic loading. *Engineering Geology* 276, 105756.

Holmes, A. 1978. *Principles of physical geology*. 3rd Ed., revised by Doris Holmes.) Wiley, New York.

Indraratna, B. & Salim, W. 2002. Modelling of particle breakage of coarse aggregates incorporating strength and dilatancy. *Proceedings of the Institution of Civil Engineers-Geotechnical Engineering* 155(4), 243-252.

Kan, M.E. and Taiebat, H.A. 2014. A bounding surface plasticity model for highly crushable granular materials. *Soils and Foundations* 54(6), 1188-1201.

Kikumoto, M., Wood, D.M. and Russell, A. 2010. Particle crushing and deformation behaviour. *Soils and Foundations* 50(4), 547-563.

Lade, P.V., Yamamuro, J.A. and Bopp, P.A. 1996. Significance of particle crushing in granular materials. *Journal of Geotechnical and Geoenvironmental Engineering, ASCE* 122(4), 309-316.

Lehane, B.M., Carraro, J.A.H., Boukpeti, N. and Elkhatib, S. 2014. Mechanical response of two carbonate sediments from Australia's North West Shelf. *33rd International Conference on Ocean, Offshore and Arctic Engineering*, 2014, Vol 3.

Liu, H.B. and Zou, D.G. 2013. Associated generalized plasticity framework for modeling gravelly soils considering particle breakage. *Journal of Engineering Mechanics, ASCE* 139(5), 606-615.

Liu, H.B., Zeng, K.F. and Zou, Y. 2020. Particle breakage of calcareous sand and its correlation with input energy. *International Journal of Geomechanics* 20(2).

Luzzani, L. and Coop, M. R. 2002. On the relationship between particle breakage and the critical state of sands. *Soils and Foundations* 42(2), 71-82.

Miura, N. and Sukeo, O. 1979 Particle-crushing of a decomposed granite soil under shear stresses. *Soils and Foundations* 19(3), 1-14.

Rowe, P.W. 1962. The stress-dilatancy relation for static equilibrium of an assembly of particles in contact. *Proceedings of the Royal Society of London. Series A. Mathematical and Physical Sciences* 269(1339), 500-527.

Shahnazari, H. and Rezvani, R. 2013. Effective parameters for the particle breakage of calcareous sands: An experimental study. *Engineering Geology* 159, 98-105.

Sharma, S.S. and Ismail, M.A. 2006. Monotonic and cyclic behavior of two calcareous soils of different origins. *Journal of Geotechnical and Geoenvironmental Engineering, ASCE* 132(12), 1581-1591.

Simoni, A. and Houlsby, G.T. 2006. The direct shear strength and dilatancy of sand–gravel mixtures. *Geotechnical & Geological Engineering* 24(3), 523.

Teng, Y., Stanier, S.A. and Gourvenec, S.M. 2019. Mechanisms beneath rectangular shallow foundations on sands: vertical loading. *Géotechnique* 70(12), 1083-1093.

Ueng, T.-S. and Lee, C.-J. 1990. Deformation behavior of sand under shear—particulate approach. *Journal of Geotechnical Engineering, ASCE,* 116(11), 1625-1640.

Ueng, T.S. and Chen, T.J. 2000. Energy aspects of particle breakage in drained shear of sands. *Géotechnique* 50(1), 65-72.

Wang, G., Wang, Z., Ye, Q. and Wei, X. 2020. Particle breakage and deformation behavior of carbonate sand under drained and undrained triaxial compression. *International Journal of Geomechanics, ASCE* 20(3).

Wang, X., Zhu, C.Q., Wang, X.Z. and Qin, Y. 2019. Study of dilatancy behaviors of calcareous soils in a triaxial test. *Marine Georesources & Geotechnology* 37(9), 1057-1070.

Watson, P., Bransby, F., Delimi, Z.L., Erbrich, C., Randolph, M., Rattley, M., Silva, M., Stevens, B., Thomas, S. and Westgate, Z. 2019. Foundation design in offshore carbonate sediments–building on knowledge to address future challenges. *In From Research to Applied Geotechnics: Invited Lectures of the XVI Pan-American Conference on Soil Mechanics and Geotechnical Engineering (XVI PCSMGE), 17-20 November 2019, Cancun, Mexico.)* IOS Press, 7, 240.

Wei, H.Z., Zhao, T., He, J.Q., Meng, Q.S. and Wang, X.Z. 2018. Evolution of particle breakage for calcareous sands during ring shear tests. *International Journal of Geomechanics, ASCE* 18(2).

Xiao, Y., Liu, H.L., Chen, Q.S., Ma, Q.F., Xiang, Y.Z. and Zheng, Y.R. 2017. Particle breakage and deformation of carbonate sands with wide range of densities during compression loading process. *Acta Geotechnica* 12(5), 1177-1184.

Xiao, Y., Liu, H.L., Ding, X.M., Chen, Y.M., Jiang, J.S. and Zhang, W.G. 2016. Influence of particle breakage on critical state line of rockfill material. *International Journal of Geomechanics, ASCE* 16(1).

Yu, F.W. 2017a. Particle breakage and the drained shear behavior of sands. *International Journal of Geomechanics, ASCE* 17(8), 04017041.

Yu, F.W. 2017b. Stress-silatancy behavior of sand incorporating particle breakage. *Acta Geotechnica Slovenica* 14(1), 55-61.

Yu, F.W. 2018. Particle breakage and the undrained shear behavior of sands. *International Journal of Geomechanics, ASCE* 18(7).

Yu, F.W. 2019. Influence of particle breakage on behavior of coral sands in triaxial tests. *International Journal of Geomechanics, ASCE* 19(12).

Zhang, H., Luo, Z., Qiu, Y., Liu, H., Gu, J. and Tang, J. 2020. Experimental and mathematical modeling of monotonic behavior of calcareous sand. *Advances in Civil Engineering* 2020.

Zhang, J.R. and Luo, M.X. 2020. Dilatancy and critical state of calcareous sand incorporating particle breakage. *International Journal of Geomechanics, ASCE* 20(4).

Zhou, A., Tao, J., Gu, X. and Hu, L. 2018. A breakage matrix model for calcareous sands subjected to one-dimensional compression. *Proceedings of GeoShanghai 2018 International Conference: Fundamentals of Soil Behaviours*.